Environmental Science & Technology

pubs.acs.org/est

Article

Real-Time Detection of Urban Atmospheric Micro−Nanoplastics and Their Chemical Mixing State Using Bioaerosol Single-Particle Mass Spectrometry

Chongchong Zhang, Yiming Qin,* Lei Li, Eleonora Aruffo, Shaoyong Li, Xuan Li, Ning Zhang, Yun Wu, Haiwei Li, Yunjiang Zhang, Yuan Dai, Ming Wang, Xinlei Ge, Ke Li, Wei Du, Chunlei Cheng, Mei Li, Mindong Chen, and Junfeng Wang*

Cite This: https://doi.org/10.1021/acs.est.5c06513

Read Online

ACCESS | Metrics & More | Article Recommendations | Supporting Information

ABSTRACT: Atmospheric micro−nanoplastics (MNPs) serve as key vectors for the global dispersion of plastic pollutants and act as reactive interfaces for atmospheric species, modifying their physicochemical properties and influencing environmental transport dynamics. However, existing methods lack the temporal resolution and specificity to characterize MNP mixing states and pollutant interactions in real time. To address this gap, we developed an innovative approach employing bioaerosol single-particle mass spectrometry (Bio-SPAMS) for simultaneous detection of polystyrene MNPs (PS MNPs; 0.3−2 μm) and their chemical associations with co-pollutants. Three diagnostic tracer ions, $^{91}[C_7H_7^+]$, $^{104}[C_8H_8^+]$, and $^{115}[C_9H_7^+]$, were identified as unambiguous markers of PS MNPs, enhancing their discrimination from ambient aerosols. Field measurements in a Chinese megacity revealed that PS MNPs constitute 1.04% of total aerosols (n = 51 045 particles), predominantly within the 0.3−0.8 μm size range. Approximately 76.4% of PS MNPs exhibited co-detection of nitrate and sulfate signatures, and in particles with PS characteristics, the relative peak areas of nitrate and sulfate are 14.30 and 4.06%, respectively, demonstrating active atmospheric aging via secondary pollutant uptake. This work established a new methodology for real-time MNP tracking in atmospheric matrices, providing critical insights into their lifecycle and risks.

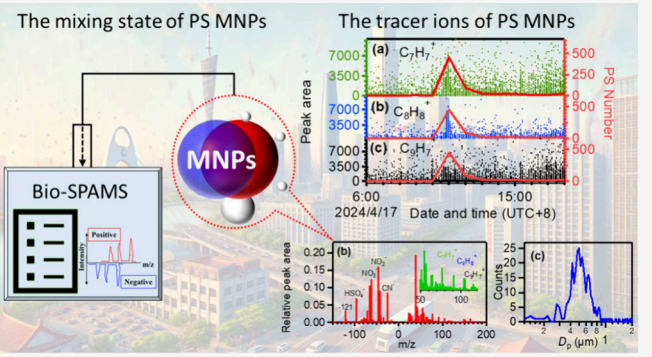

KEYWORDS: *micro−nanoplastics (MNPs), bioaerosol single-particle mass spectrometry (Bio-SPAMS), polystyrene (PS), mixing state, real-time detection*

1. INTRODUCTION

Micro−nanoplastics (MNPs) have emerged as pervasive environmental contaminants,[1−3] with atmospheric transport recognized as an important pathway for their global dispersion and human exposure.[4−8] Beyond passive carriers, airborne MNPs dynamically interact with co-existing pollutants, forming complex mixtures that influence atmospheric processes, radiative forcing, and human health.[2,7,9−16] The mixing state, defined as the molecular-scale association of MNPs with adsorbed species, critically governs their reactivity, toxicity,[17] and climatic effects.[18] For instance, microplastics have been shown to enhance the toxicity of florfenicol, an antimicrobial agent, by acting as carriers or disrupting metabolic processes.[19−22] The ice-nucleating efficiency of MNPs can also be altered upon mixing with inorganics such as sulfuric acid and ammonium sulfate,[23] which has implications for cloud formation and climate feedback. Despite this significance, real-time characterization of MNP mixing states at the single-particle level remains challenging, limiting mechanistic understanding of their atmospheric transformation and environmental effects.

Traditional methods for atmospheric MNPs analysis rely on offline techniques with inherent limitations.[24,25] Visual identification, applicable only to millimeter-scale (1−5 mm) plastics, lacks the ability to identify polymer types or distinguish plastics from organics, and introduces observer bias.[26] Fourier transform infrared (FTIR) and Raman spectroscopies resolve polymer types but suffer from diffraction limits (>10 μm resolution), environmental interference, and throughput constraints.[7,27−30] Bulk mass spectrometry (MS) methods including pyrolysis−gas chromatography−

Received: May 22, 2025
Revised: September 13, 2025
Accepted: September 15, 2025

mass spectrometry (Pyr−GC−MS), thermal desorption−gas chromatography−mass spectrometry (TDS−GC−MS), and matrix-assisted laser desorption/ionization time-of-flight mass spectrometry (MALDI−TOF MS), provide chemical specificity but require destructive sample processing, altering native particle morphologies and masking real-time interaction dynamics.[7,26,31−34] While Aerodyne high-resolution time-of-flight aerosol mass spectrometry (HR-ToF-AMS) enables real-time detection of sub-micrometer polystyrene (PS) and polyethylene terephthalate (PET) particles (0.05−1.0 μm),[35,36] its design fundamentally restricts mixing state analysis: aerodynamic focusing and high-temperature vaporization (600 °C) at the tungsten surface homogenize particle components and ionized by electron ionization (70 eV), precluding single-particle speciation.[37−40] In contrast, single-particle aerosol mass spectrometry (SPAMS) overcomes these limitations by coupling aerodynamic sizing with dual-polarity time-of-flight detection.[40,41] Using laser desorption/ionization, it vaporizes the entire particle and detects core and associated species via time-of-flight mass spectrometry. This enables direct identification of internally mixed components, distinguishing particles with complex chemical associations from externally mixed ones.[42−46]

This study pioneers the application of Bio-SPAMS for *in situ* chemical characterization of polystyrene micro−nanoplastics (PS MNPs) and their atmospheric mixing states. We analyzed both laboratory-generated PS MNPs and ambient aerosols sampled in urban Guangzhou, China. Co-detection of sulfate and nitrate on most of PS MNPs reveals rapid atmospheric aging, forming chemically complex aerosols that may modulate atmospheric reactivity, particle nucleation processes, and toxicity profiles. These findings would provide critical parametrizations for atmospheric models, specifically, MNP number concentrations, size-resolved aging rates, and surface uptake coefficients, enabling robust assessment of their climate and health impacts.

2. EXPERIMENTAL METHODS

The Bio-SPAMS (Nanjing Feng-Sun Intelligent Technology Co., Ltd., China) were employed in all the laboratory experiments and ambient sampling of this study. The Bio-SPAMS is developed based on the SPAMS[47,48] and is primarily composed of control and acquisition software, a sampling system, a diameter measurement system, an ionization system, and a mass spectrometry system to characterize aerosol particle size and chemical composition at the single-particle level.

The instrument employs aerodynamic lenses to focus aerosol particles into a particle beam for introduction into a vacuum chamber. The focused particle beam subsequently traverses two continuous-wave (CW) diode-pumped neodymium-doped yttrium aluminum garnet (Nd:YAG) laser beams (λ = 532 nm) for real-time aerodynamic sizing of individual particles via light scattering. Following sizing, particles are precisely positioned within the ionization source chamber, where a pulsed Nd:YAG laser (λ = 266 nm) generates simultaneous positive and negative ion fragments through photoionization and dissociative electron processes. The ionized products are then detected using a dual-polarity time-of-flight mass spectrometer (dual TOF-MS), enabling the measurement of distinct chemical components within individual aerosol particles. The system's design principles are detailed in the literature by Du et al.[47] and Li et al.[48]

Prior to sampling, the Bio-SPAMS requires particle size calibration and mass spectrometry calibration, with detailed calibration procedures provided in Text S1, and the sampling flow rate was set at 0.35 L min^{-1}, while the ionization laser energy was adjusted under exploratory conditions, as detailed in section 3.2. The chemical composition and particle sizes of single particles collected by the SPAMS were analyzed using MATLAB and the Version 1.3 of Computational Continuation Core (COCO V1.3).[46] In this study, the programs of "averaged and digitized spectra", "particle size distribution", and "search for particles with specific conditions" were mainly used for data analysis.

The HR-TOF-AMS (Aerodyne Research, Inc., U.S.A.) was conducted parallelly to measure the total concentration of PS NNPs, as reported by Niu et al.[35] The working principle of the HR-TOF-AMS is extensively detailed in the studies by Decarlo et al.[49] and Jayne et al.[38] Ionization efficiency (IE) and particle size calibration were performed in accordance with the protocols outlined by Canagaratna et al.[50] and Drewnick et al.[40] In this study, particles were sampled at a flow rate of 1.43 cm^3 s^{-1}, vaporized at approximately 600 °C, with the mass spectrometer operating in V-mode.[51] The HR-ToF-AMS data set was analyzed by using the Igor-based standard ToF-AMS Analysis Toolkit SOUIRREL v1.59D and PIKAv1.19D (https://cires1.colorado.edu/jimenez-group/wiki/index.php?title=ToF-AMS_Main).

To acquire the standard mass spectrum of pure PS MNP, an aqueous solution of 500 nm monodispersed PS particles (Thermo Scientific, 8 wt %) was generated by a constant-output atomizer (TSI, Inc., model 9302), and concurrently analyzed by both Bio-SPAMS and HR-ToF-AMS. The sampling was stopped after 5000 mass spectra were acquired by the Bio-SPAMS. The experimental setup is depicted in Figure 1a.

The laser energy and particle size were further tested to evaluate the influence of different conditions on PS MNPs using Bio-SPAMS. The optimization of laser energy was investigated by testing six discrete energy levels (300−1550 μJ; Table S1) at a constant particle size of 500 nm. Particle size-dependent collection efficiency was evaluated by analyzing PS

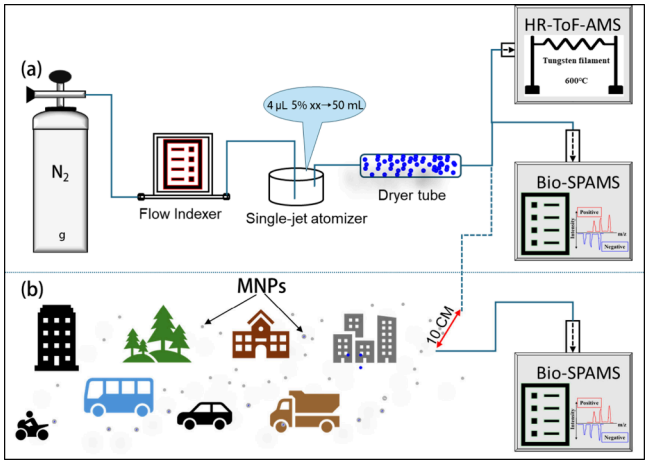

Figure 1. Schematic of the experimental setup: (a) experimental setup for laboratory aerosol generation and detection and (b) experimental setup for ambient aerosol detection with standard PS ("10 CM" in panel b refers to the distance from the spray nozzle to the sampling inlet).

https://doi.org/10.1021/acs.est.5c06513
Environ. Sci. Technol. XXXX, XXX, XXX−XXX

MNPs (Thermo Scientific, 8 wt %) ranging from 0.3 to 2 μm within the optimized laser energy range, at ~380 μJ based on prior optimization. The specific experiment involved aerosolizing an aqueous solution containing pure monodisperse PS particles using the atomizer, followed by collection and analysis with Bio-SPAMS (Figure 1a).

To assess the capability of detecting mixed states, a mixed solution was aerosolized using the atomizer and collected by Bio-SPAMS within the optimized laser energy range. The mixed solution was prepared by combining 500 nm PS MNPs with equal volumes of ammonium sulfate (AS, 8 wt %, 4 μL) and sodium nitrate (SN, 8 wt %, 4 μL) in ultrapure water. To distinguish PS MNP-specific signals from potential interferents, comparative analyses were conducted using literature-derived data, and incense combustion was detected by Bio-SPAMS within the optimized laser energy range. Detailed findings are presented in section 3.3. The experimental processes are detailed in Text S2.

Ambient aerosol samples were collected over a 3 day period in Huangpu District, Guangzhou, a megacity characterized by a large permanent population and intensive plastic consumption, to investigate particulate matter composition under high anthropogenic influence. During sampling, the 500 nm PS through the experimental procedures of Figure 1a was sprayed into the air 3 times (under normal ventilation conditions), each time for 5 min, and the spray experiments were conducted in a well-ventilated outdoor, ventilated environment. This spray port is 10 cm from the sampling port (Figure 1b), and the sampling port is about 9 m above the ground.

3. RESULTS AND DISCUSSION

3.1. Mass Spectrum of Pure PS MNP Standard. The mass spectral signatures of pure PS MNPs obtained via Bio-SPAMS were compared with parallel measurements using HR-ToF-AMS to evaluate detection capabilities (Figure 2). The

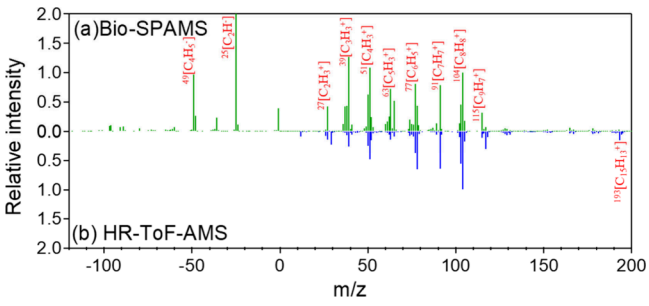

Figure 2. Mass spectra of PS MNPs detected by Bio-SPAMS and HR-TOF-AMS: (a) mass spectra of pure PS by Bio-SPAMS and (b) mass spectra of pure PS by HR-ToF-AMS (relative intensities obtained in terms of peak area or concentration of $C_8H_8^+$).

mass spectrum of pure PS MNPs using Bio-SPAMS at 384.24 ± 5.68 μJ revealed a fragmentation profile dominated by hydrocarbon ions ($^n[C_xH_y^{\pm}]$) (Figure 2a), including m/z $^{25}[C_2H^-]$, $^{49}[C_4H_5^-]$, $^{39}[C_3H_3^+]$, $^{51}[C_4H_3^+]$, $^{63}[C_5H_5^+]$, $^{77}[C_6H_5^+]$, $^{91}[C_7H_7^+]$, $^{104}[C_8H_8^+]$, and $^{115}[C_9H_7^+]$, which is mostly consistent with the aromatic−aliphatic backbone. Compared with Bio-SPAMS (Figure 2a), the results by HR-ToF-AMS align with the positive mass spectrum by Bio-SPAMS, which detected analogous ions in Figure 2b (m/z $^{39}[C_3H_3^+]$, $^{51}[C_4H_3^+]$, $^{63}[C_5H_5^+]$, $^{77}[C_6H_5^+]$, $^{91}[C_7H_7^+]$, $^{104}[C_8H_8^+]$, $^{115}[C_9H_7^+]$, and $^{193}[C_{15}H_{13}^+]$), are consistent with previous results[35] as well as the mass spectra of styrene in the NIST library, confirming PS MNPs identifiable spectral fingerprints across both methods. Bio-SPAMS is also able to capture aliphatic fragments in negative ion mode (m/z $^{25}[C_2H^-]$ and $^{49}[C_4H_5^-]$). The m/z 104 peak ($^{104}[C_8H_8^+]$), corresponding to styrene monomer release, was consistently observed in both methods but exhibited higher relative intensity in Bio-SPAMS. These findings demonstrate that Bio-SPAMS can detect PS MNPs through characteristic spectral fingerprints. However, the complete mass spectrometry of PS still needs to be further explored and, experimental conditions also need to be further optimized, since the detection results by Bio-SPAMS are affected by the laser energy, the particle size, and the composition.[47,52,53]

3.2. Optimized Detection Conditions. To optimize the detection conditions for PS MNPs using Bio-SPAMS, we further investigated the effects of laser energy and particle size on detection efficiency and mass spectral completeness (Figure 3 and Figures S1 and S2).

3.2.1. Impact of Laser Energy on Detection Performance. Laser energy is a key parameter influencing both the ionization efficiency and the fragmentation pattern of aerosol particles. Thus, we conducted experiments detecting 500 nm PS MNPs at six laser energy levels (300−1550 μJ) (Table S1) by Bio-SPAMS, collecting 5000 mass spectra at each setting. The average mass spectra for each laser energy is presented in Figure S1 of the Supporting Information. The results revealed that increasing laser energy leads to a reduction in the signal intensity of large fragment ions in positive ion mode, e.g., $^{91}[C_7H_7^+]$, $^{104}[C_8H_8^+]$, and $^{115}[C_9H_7^+]$ (Figure 3a and Figure S1), while in negative ion mode, although the variety of fragment ions increases, the signal strength of key ions, e.g., $^{25}[C_2H^-]$ and $^{49}[C_4H_5^-]$ diminishes (Figure S1). This observation aligns with previous studies Silva and Prather,[54] which reported that higher laser energies promote further fragmentation of large ions into smaller species. Thus, lower laser energies are more effective for preserving large fragment ions, which are critical for identifying target compounds.[55,56]

Since there is no standard mass spectral library for laser ionization resolution, but according to the existing research results, molecular ions generally occur at low laser energies.[47,54] Therefore, it can be known a more complete mass spectrum of PS MNPs can be obtained in the range of laser energies from 301.87 ± 6.12 to 635.61 ± 33.11 μJ, because the large ion fragment $C_9H_7^+$ has remained present under the range of laser energy (301.87 ± 6.12 to 635.61 ± 33.11 μJ) (Figure 3a and Figure S1). Although a more complete mass spectrum of PS MNPs can be obtained in the range of laser energies from 301.87 ± 6.12 to 635.61 ± 33.11 μJ, the detection efficiency (including hit rate) at different laser energies still needs to be considered in the experiment.[47]

The hit rate reaches the stable highest level of about 96.89−98.72% between 635.61 ± 33.11 and 1200 μJ (Figure 3a). However, when laser energy exceeds 635.61 ± 33.11 μJ, the signals for critical ions such as $C_7H_7^+$, $C_8H_8^+$, and $C_9H_7^+$ (Figure 3a) nearly disappeared. Previous studies have demonstrated that excessive laser energy can lead to non-specific fragmentation and reduced ionization efficiency for specific compounds.[47,54] To balance the retention of key fragment ions with a high hit rate, the recommended laser energy range should be maintained above 301.87 ± 6.12 μJ and kept below 635.61 ± 33.11 μJ for optimal performance. Li

https://doi.org/10.1021/acs.est.5c06513
Environ. Sci. Technol. XXXX, XXX, XXX−XXX

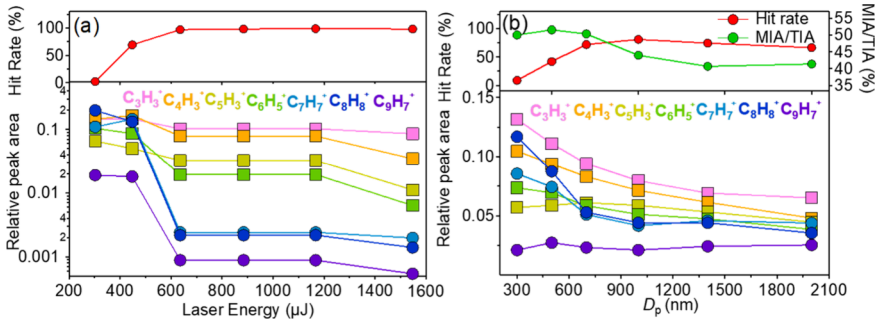

Figure 3. PS was detected by Bio-SPAMS: (a) detection efficiency of 500 nm PS MNPs at different laser energies and (b) detection efficiency of PS MNPs at different sizes (MIA, major ion abundance stands for total relative peak areas of major ions; TIA, total ion abundance stands for total relative peak area of total ions; MIA/TIA, major ion abundance to total ion abundance ratio; and MIA/TIA enables quantitative assessment of the proportion of major target ions within total ionization products).

et al.[48] have reported that a pulsed 266 nm Nd:YAG laser (Ultra Quantel, France) with adjustable energy from 0.1 to 10 mJ is commonly used for particle ionization, a energy range of 301.87 to 635.61 μJ falls well within this operational window. This range ensures sufficient ionization while minimizing excessive fragmentation, there by preserving the characteristic spectral fingerprints of PS MNPs.

3.2.2. Impact of Particle Size on Detection Efficiency. Particle size is another critical factor influencing the performance.[47,57] Thus, we detected PS MNPs of six sizes (300 nm, 500 nm, 700 nm, 1 μm, 1.4 μm, and 2 μm) under the same optimized laser energy range (above 301.87 ± 6.12 μJ and below 635.61 ± 33.11 μJ) by Bio-SPAMS. The results confirm that PS MNPs across the 0.3 to 2 μm size range can be effectively detected by Bio-SPAMS, with consistent identification of key fragment ions (e.g., C_2H^-, $C_4H_5^-$, $C_3H_3^+$, $C_4H_3^+$, $C_5H_5^+$, $C_6H_5^+$, $C_7H_7^+$, $C_8H_8^+$, and $C_9H_7^+$), as observed in Figures 2a and 3a.

However, the relative peak areas of key fragment ions varied across different particle sizes (Figure S2 and Figure 3b). For instance, 500 and 700 nm PS MNPs exhibited significantly higher relative peak areas for C_2H^-, while 300 and 500 nm PS MNPs showed greater relative peak areas for $C_8H_8^+$. Moreover, we also calculated the ratio of the total relative peak area of major ions to that of all ions (MIA/TIA) to evaluate detection efficiency comprehensively. The 500 nm PS MNPs demonstrated the highest MIA/TIA ratio (51.54%), indicating superior detection efficiency for key fragment ions. Additionally, 500 nm PS MNPs achieved the highest hit rate of 80.88% (Figure 3b). These results suggest that 500 nm PS MNPs are optimal for experimental detection, as they provide a balance between signal intensity and detection efficiency.

Therefore, the optimal conditions for detecting PS MNPs with Bio-SPAMS are achieved by adjusting the laser energy to between 301.87 ± 6.12 and 635.61 ± 33.11 μJ, which balances the preservation of key fragment ions with a high hit rate. Additionally, particle sizes between 500 and 700 nm maximize detection efficiency and ensure high spectral integrity. The mass spectra obtained from Bio-SPAMS under the aforementioned optimal conditions (Figure 2a) were selected as the standard spectra (fingerprint) for subsequent studies.

3.3. Identification of PS MNP Tracer Ions. To accurately extract PS MNPs from complex environmental samples, it is essential to identify unique tracer ions that can distinguish PS MNPs from interfering species. Previous studies have highlighted the challenges of detecting MNPs in atmospheric matrices due to potential interferences from structural similarities in organic components[58] such as organic carbon (OC),[44,57] biomass burning (BB),[44,57−60] and polycyclic aromatic hydrocarbons (PAHs).[61,62] These substances can produce ions similar to PS MNPs, complicating the detection process.

Thus, we further analyzed the mass spectra of PS MNPs and potential interferents to identify characteristic tracer ions. As shown in Table S2, common interfering ions, e.g., $^{25}[C_2H^-]$, $^{49}[C_4H_5^-]$, $^{39}[K^+]$, $^{51}[C_4H_3^+]$, $^{63}[C_5H_5^+]$, and $^{77}[C_6H_5^+]$ primarily originate from OC, BB, and PAHs. To exclude these interferences, we focused on ions that are unique to PS MNPs. Our results demonstrated that $^{91}[C_7H_7^+]$, $^{104}[C_8H_8^+]$ and $^{115}[C_9H_7^+]$ do not appear simultaneously in the mass spectra of burning incense (Figure 4) (biomass burning

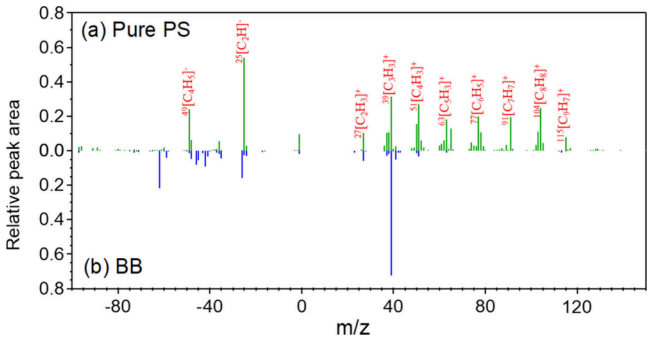

Figure 4. Mass spectra of pure PS and incense burning particles: (a) mass spectra of pure 500 nm PS under optimized energy conditions and (b) mass spectra of the burning incense under optimized energy conditions.

organic aerosol, BB) and standard PAHs[62] at 500 μJ by SPAMS. Thus, $C_7H_7^+$, $C_8H_8^+$ and $C_9H_7^+$ can be considered as tracer ions for PS MNPs from laser ionization at an energy between 301.87 ± 6.12 and 635.61 ± 33.11 μJ by Bio-SPAMS.

3.4. Identification of Mixing States of PS MNPs with Other Components. We conducted experiments by mixing standard 500 nm PS MNPs with common inorganic substances, specifically ammonium sulfate (AS) and sodium nitrate (SN). An average mass spectrum of 5000 single particles from a mixture of PS, AS, and SN, collected by the Bio-SPAMS is shown in Figure 5. Compared with the mass spectra of pure PS MNPs (Figure 5a), the mass spectra of the mixture exhibit clear signals for nitrate and sulfate ions (Figure 5a), the relative intensity of nitrate (m/z $^{62}[NO_3^-]$, $^{46}[NO_2^-]$,

https://doi.org/10.1021/acs.est.5c06513
Environ. Sci. Technol. XXXX, XXX, XXX−XXX

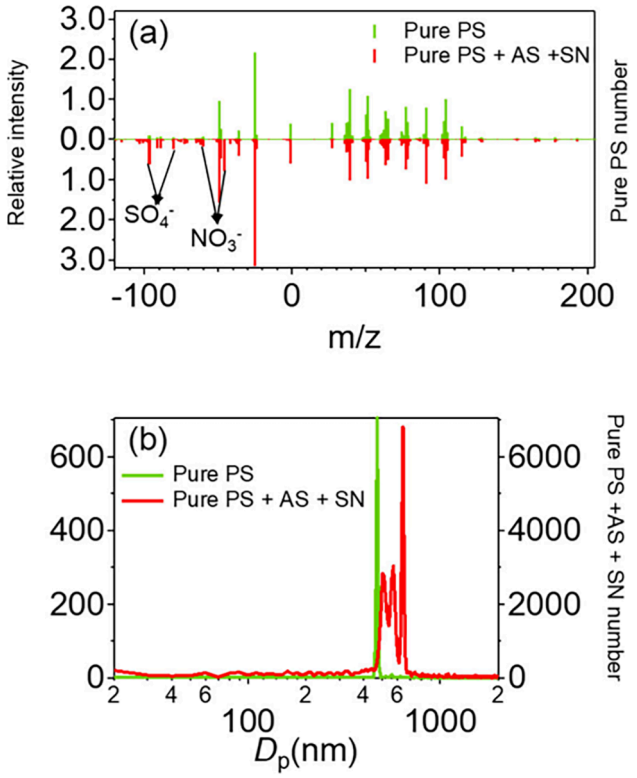

Figure 5. PS internally mixed with common inorganics: (a) mass spectra of pure 500 nm PS, (b) mass spectra of mixture (sodium nitrate, ammonium sulfate, and PS MNPs), and (c) particle size distribution of mixture (sodium nitrate, ammonium sulfate, and PS MNPs) (relative intensity obtained in terms of peak area of $C_8H_8^+$).

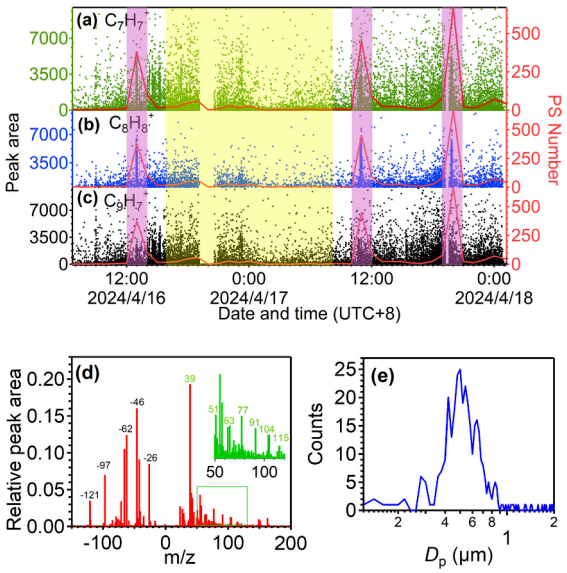

Figure 6. Ambient measurement of PS with Bio-SPAMS in an urban environment in Guangzhou: (a, b, and c) peak area of $^{91}[C_7H_7^+]$, $^{104}[C_8H_8^+]$, and $^{115}[C_9H_7^+]$ in the ambient aerosol and the change of PS MNPs searched (each purple-shaded area is the time period when the standard PS was sprayed into the atmosphere for 5 min, and the yellow-shaded region is the time periods of the ambient aerosol), (d) mass spectra of particles characterized as PS were detected in the yellow-shaded region, and (e) particle size distribution of particles characterized as PS were detected in the yellow-shaded region.

and $^{30}[NO^-]$) is about 0.94 and that of sulfate(m/z $^{97}[HSO_4^-]$, $^{96}[SO_4^-]$, $^{81}[HSO_3^-]$, and $^{80}[SO_3^-]$) is about 1.46 in mass spectra of mixture, while in mass spectra of pure, the relative intensity of nitrate is about 0.027 and that of sulfate is about 0.23. Furthermore, the particle size distribution of the mixture showed a broader range, with most particles exceeding 500 nm (Figure 5b). This increase in particle size suggests that PS MNPs may be in a state of embedment or surface adsorption with sulfate and nitrate.[15] These results indicate that our method can identify the mixing state of MNPs with the co-existing species at the individual particle level.

3.5. Validation and Application to the Detection of Atmospheric PS. Atmospheric aerosol samples with labeled PS MNPs (500 nm) were collected by Bio-SPAMS under optimized conditions (laser energy: 410.85 ± 6.06 μJ) from April 15 to 18, 2024. A total of 122 348 particles with mass spectra were collected. Using $^{91}[C_7H_7^+]$, $^{104}[C_8H_8^+]$, and $^{115}[C_9H_7^+]$ as qualitative fragment ions, we applied a relative peak area threshold of ≥0.005 for $^{104}[C_8H_8^+]$ based on Zhang et al.[62] and ion signal intensity. This threshold, well above baseline levels, minimized background noise interference and ensured reliable detection of low-abundance MNPs. Under these criteria, 3198 particles exhibiting PS MNP characteristics were identified, representing 2.61% of total particles. Time-series analysis revealed a clear correlation between the release of standard PS MNPs into the atmosphere and the detected number of PS MNP-like particles (Figure 6a–c). During the periods when labeled PS MNPs were introduced, the peak areas of $^{91}[C_7H_7^+]$, $^{104}[C_8H_8^+]$, and $^{115}[C_9H_7^+]$ showed a significant increase, especially, the changes in the peak area of $^{104}[C_8H_8^+]$ are more synchronized with the changes in the quantity of labeled PS MNPs, confirming the reliability of these tracer ions in extracting PS MNPs from complex environmental matrices.

A total number of 51 045 ambient aerosols without labeled PS MNPs collected for 27.5 h by Bio-SPAMS (yellow-shaded regions in Figure 6a, b, and c) demonstrated that PS MNPs accounted for approximately 1.04% of the total detected particles (Figure 6d and e). Notably, 76.42% of these PS MNPs exhibited strong signals for nitrate and sulfate (e.g., m/z $^{97}[HSO_4^-]$, $^{96}[SO_4^-]$, $^{81}[HSO_3^-]$, and $^{80}[SO_3^-]$ and m/z $^{62}[NO_3^-]$, $^{46}[NO_2^-]$, and $^{30}[NO^-]$), and in particles with PS characteristics, the relative peak area of nitrate and sulfate are 14.30 and 4.06%, respectively (Figure 6d), these findings suggest that PS MNPs may interact with co-existing inorganic pollutants. The particle size is mainly concentrated in the range of 0.3–0.8 μm (Figure 6e). Thus, microplastics may act as carriers for other pollutants, enhancing their environmental persistence and transportability.[15]

The results showed that the content of PS MNPs about 0.3–0.8 μm was significantly lower than that of conventional pollutants in the atmosphere in Guangzhou. Similarly, the results of Niu et al. also showed that the mass concentration of PS NPS in the atmosphere of Texas was 30 ± 20 ng m^{-3} by HR-TOF-AMS, which was lower than that of conventional pollutants.[35] Kirchsteiger et al.[63] reported that in Graz, Austria, the microplastic content was 0.67% of $PM_{2.5}$ by thermal desorption proton transfer reaction mass spectrometry (TD–PTR–MS). This indicates that the current atmospheric content of MNPs remains at an extremely low level compared to conventional pollutants such as sulfates, nitrates, black carbon, and mineral dust.

https://doi.org/10.1021/acs.est.5c06513
Environ. Sci. Technol. XXXX, XXX, XXX–XXX

However, the low concentration of MNPs does not equate to negligible environmental impacts. Due to their strong environmental persistence and global cycling capacity, MNPs may accumulate invisibly, and their potential risks could manifest through complex interactions with other pollutants in the atmosphere.[1] This suggests that some other air contaminants can interfere with the detection of PS MNPs (e.g., masking the signal from PS MNPs, wrapping around the surface of PS MNPs, etc.). Besides, the particles with PS characteristics, also have extremely strong nitrate and sulfate signals, which may be due to their surface properties (e.g., charge distribution and functional group formation), environmental conditions (e.g., humidity), and interaction with other particulate matter.[64]

4. ATMOSPHERIC IMPLICATIONS

This study achieved real-time, single-particle identification of PS MNPs in urban aerosols through diagnostic tracer ions: $^{91}[C_7H_7^+]$, $^{104}[C_8H_8^+]$, and $^{115}[C_9H_7^+]$, which provide unambiguous differentiation from organic/inorganic interferents using Bio-SPAMS. Systematic optimization of desorption/ionization parameters revealed an operational laser energy window of 301.87 ± 6.12 to 635.61 ± 33.11 μJ. Within this range, PS MNPs (500−700 nm) exhibited maximal detection efficiency and reproducible fragmentation patterns. Field measurements in urban Guangzhou quantified PS MNPs at 1.04% of ambient aerosols, most of them were in the 0.3−0.8 μm size range. These findings highlight the predominance of respirable nanoplastics and underscore the necessity for submicrometer analytical resolution. In addition, approximately 76.4% of PS MNPs co-detected nitrate and sulfate enrichments, suggesting dynamic interactions with co-existing pollutants during atmospheric processing. This frequent co-detection suggests that PS MNPs undergo atmospheric aging via condensation or heterogeneous reactions with secondary inorganic aerosols. Such transformations likely enhance particle hygroscopicity, atmospheric lifetime, and deposition behavior, potentially increasing their ability to act as ice nucleating particles (INPs) or to penetrate deeper into the human respiratory tract.[19−23,65]

Importantly, the mixing state and particle size information derived from tracer ions offers a valuable foundation for the parametrization of PS MNP aging in atmospheric models. For instance, reaction rates or coating efficiencies could be constrained using observed nitrate/sulfate associations, analogous to existing schemes for soot or organic aerosol aging.[66,67] Incorporating such dynamics would improve model predictions of plastic particle transport, transformation, and deposition under variable environmental conditions.[66−68] Overall, this study bridges analytical innovation with environmental relevance by unveiling not only the presence of airborne PS MNPs in urban environments but also their chemical evolution during atmospheric processing. These insights contribute toward a mechanistic understanding of nanoplastic−pollutant interactions and facilitate their integration into multiscale models that address aerosol−climate−health linkages. In the context of global change, the dynamic behavior of airborne MNPs deserves increased attention as both a novel pollutant and an active participant in the atmospheric system.

However, one limitation of this study is the potential underrepresentation of particles smaller than 300 nm and larger than 1 μm. The former is challenging to detect due to their low mass, which results in weak ion signals and inefficient laser ionization, while the latter may be lost because of aerodynamic lens transmission inefficiencies[69] and sampling losses. These size ranges are environmentally relevant: sub-300 nm particles tend to be more bioavailable, whereas coarse particles (>1 μm) can carry higher loads of sorbed pollutants. To address this gap, future research should focus on enhancing the sensitivity and transmission efficiency of single-particle mass spectrometry platforms, enabling more comprehensive detection and characterization across the full size spectrum of atmospheric MNPs.

■ ASSOCIATED CONTENT

Supporting Information

The Supporting Information is available free of charge at https://pubs.acs.org/doi/10.1021/acs.est.5c06513.

Instrument description and calibration of Bio-SPAMS (Text S1), preparation of laboratory-generated aerosol samples and cleaning protocols (Text S2), mass spectra of PS at different laser energies (Figure S1), mass spectra of PS at different particle sizes (Figure S2), six different laser energies (Table S1), and ion markers for different particle types measured by SPAMS (Table S2) (PDF)

■ AUTHOR INFORMATION

Corresponding Authors

Yiming Qin − *School of Energy and Environment, City University of Hong Kong, Hong Kong 999077, China;* orcid.org/0000-0002-1552-5139; Email: ymqin3@cityu.edu.hk

Junfeng Wang − *Jiangsu Key Laboratory of Atmospheric Environment Monitoring and Pollution Control (AEMPC), Collaborative Innovation Center of Atmospheric Environment and Equipment Technology (CIC-AEET), School of Environmental Science and Engineering and School of Emergency Management, Nanjing University of Information Science and Technology, Nanjing 210044, China;* Email: wangjunfeng@nuist.edu.cn

Authors

Chongchong Zhang − *Jiangsu Key Laboratory of Atmospheric Environment Monitoring and Pollution Control (AEMPC), Collaborative Innovation Center of Atmospheric Environment and Equipment Technology (CIC-AEET), School of Environmental Science and Engineering, Nanjing University of Information Science and Technology, Nanjing 210044, China;* orcid.org/0000-0002-6835-7829

Lei Li − *College of Environment and Climate, Institute of Mass Spectrometry and Atmospheric Environment, Jinan University, Guangzhou 510632, China*

Eleonora Aruffo − *Department of Advanced Technologies in Medicine & Dentistry, University "G.d'Annunzio" of Chieti-Pescara, Chieti 66100, Italy; Center for Advanced Studies and Technology (CAST), Chieti 66100, Italy;* orcid.org/0000-0002-9164-7293

Shaoyong Li − *College of Environment and Climate, Institute of Mass Spectrometry and Atmospheric Environment, Jinan University, Guangzhou 510632, China*

Xuan Li − *College of Environment and Climate, Institute of Mass Spectrometry and Atmospheric Environment, Jinan University, Guangzhou 510632, China*

https://doi.org/10.1021/acs.est.5c06513
Environ. Sci. Technol. XXXX, XXX, XXX−XXX

Ning Zhang − *Jiangsu Key Laboratory of Atmospheric Environment Monitoring and Pollution Control (AEMPC), Collaborative Innovation Center of Atmospheric Environment and Equipment Technology (CIC-AEET), School of Environmental Science and Engineering, Nanjing University of Information Science and Technology, Nanjing 210044, China*

Yun Wu − *Jiangsu Key Laboratory of Atmospheric Environment Monitoring and Pollution Control (AEMPC), Collaborative Innovation Center of Atmospheric Environment and Equipment Technology (CIC-AEET), School of Environmental Science and Engineering, Nanjing University of Information Science and Technology, Nanjing 210044, China*

Haiwei Li − *Jiangsu Key Laboratory of Atmospheric Environment Monitoring and Pollution Control (AEMPC), Collaborative Innovation Center of Atmospheric Environment and Equipment Technology (CIC-AEET), School of Environmental Science and Engineering, Nanjing University of Information Science and Technology, Nanjing 210044, China*

Yunjiang Zhang − *Jiangsu Key Laboratory of Atmospheric Environment Monitoring and Pollution Control (AEMPC), Collaborative Innovation Center of Atmospheric Environment and Equipment Technology (CIC-AEET), School of Environmental Science and Engineering, Nanjing University of Information Science and Technology, Nanjing 210044, China;* orcid.org/0009-0005-8777-2082

Yuan Dai − *Jiangsu Key Laboratory of Atmospheric Environment Monitoring and Pollution Control (AEMPC), Collaborative Innovation Center of Atmospheric Environment and Equipment Technology (CIC-AEET), School of Environmental Science and Engineering, Nanjing University of Information Science and Technology, Nanjing 210044, China; Yangzhou Environmental Monitoring Center of Jiangsu Province, Yangzhou 225009, China*

Ming Wang − *Jiangsu Key Laboratory of Atmospheric Environment Monitoring and Pollution Control (AEMPC), Collaborative Innovation Center of Atmospheric Environment and Equipment Technology (CIC-AEET), School of Environmental Science and Engineering, Nanjing University of Information Science and Technology, Nanjing 210044, China*

Xinlei Ge − *School of Energy and Environment, Southeast University, Nanjing 211189, China;* orcid.org/0000-0001-9531-6478

Ke Li − *Jiangsu Key Laboratory of Atmospheric Environment Monitoring and Pollution Control (AEMPC), Collaborative Innovation Center of Atmospheric Environment and Equipment Technology (CIC-AEET), School of Environmental Science and Engineering, Nanjing University of Information Science and Technology, Nanjing 210044, China;* orcid.org/0000-0002-9181-3562

Wei Du − *Yunnan Provincial Key Laboratory of Soil Carbon Sequestration and Pollution Control, Faculty of Environmental Science & Engineering, Kunming University of Science & Technology, Kunming 650500, China;* orcid.org/0000-0001-6047-525X

Chunlei Cheng − *College of Environment and Climate, Institute of Mass Spectrometry and Atmospheric Environment, Jinan University, Guangzhou 510632, China;* orcid.org/0000-0002-4130-7936

Mei Li − *College of Environment and Climate, Institute of Mass Spectrometry and Atmospheric Environment, Jinan University, Guangzhou 510632, China*

Mindong Chen − *Jiangsu Key Laboratory of Atmospheric Environment Monitoring and Pollution Control (AEMPC), Collaborative Innovation Center of Atmospheric Environment and Equipment Technology (CIC-AEET), School of Environmental Science and Engineering, Nanjing University of Information Science and Technology, Nanjing 210044, China*

Complete contact information is available at: https://pubs.acs.org/10.1021/acs.est.5c06513

Notes

The authors declare no competing financial interest.

■ ACKNOWLEDGMENTS

This work was funded by the National Key R&D Program of China (2024YFC3714200), the National Natural Science Foundation of China (U24A20515, 22276099, and 42405095), and the Jiangsu Provincial Outstanding Youth Foundation (BK20240036). Support from the Guangxi Science and Technology Key R&D Program (AB24010074), the CityUHK Startup Grant (9610624), and Postgraduate Research & Practice Innovation Program of Jiangsu Province (KYCX25_1672) is acknowledged.

■ REFERENCES

(1) Thompson, R. C.; Courtene-Jones, W.; Boucher, J.; Pahl, S.; Raubenheimer, K.; Koelmans, A. A. Twenty years of microplastic pollution research—What have we learned? *Science* **2024**, *386* (6720), No. eadl2746.

(2) Li, C.; Liu, J.; Rillig, M. C.; Bank, M. S.; Fantke, P.; Zhu, D.; Zhu, Y.-G.; Jin, L. N. What harmful microbes are lurking in the world's 7 billion tonnes of plastic waste? *Nature* **2024**, *634* (8032), 30−32.

(3) Li, C.; Li, X.; Bank, M. S.; Dong, T.; Fang, J. K.-H.; Leusch, F. D. L.; Rillig, M. C.; Wang, J.; Wang, L.; Xia, Y.; Xu, E. G.; Yang, Y.; Zhang, C.; Zhu, D.; Liu, J.; Jin, L. The "Microplastome"—A holistic perspective to capture the real-world ecology of microplastics. *Environ. Sci. Technol.* **2024**, *58* (9), 4060−4069.

(4) Zhang, Y.; Gao, T.; Kang, S.; Allen, S.; Luo, X.; Allen, D. Microplastics in glaciers of the Tibetan Plateau: evidence for the long-range transport of microplastics. *Sci. Total Environ.* **2021**, *758*, 143634.

(5) Sridharan, S.; Kumar, M.; Singh, L.; Bolan, N. S.; Saha, M. Microplastics as an emerging source of particulate air pollution: a critical review. *J. Hazard. Mater.* **2021**, *418*, 126245.

(6) Brahney, J.; Mahowald, N.; Prank, M.; Cornwell, G.; Klimont, Z.; Matsui, H.; Prather, K. A. Constraining the atmospheric limb of the plastic cycle. *Proc. Natl. Acad. Sci. U. S. A.* **2021**, *118* (16), No. e2020719118.

(7) Luo, D.; Chu, X.; Wu, Y.; Wang, Z.; Liao, Z.; Ji, X.; Ju, J.; Yang, B.; Chen, Z.; Dahlgren, R.; Zhang, M.; Shang, X. Micro- and nano-plastics in the atmosphere: a review of occurrence, properties and human health risks. *J. Hazard. Mater.* **2024**, *465*, 133412.

(8) Xiao, S.; Cui, Y.; Brahney, J.; Mahowald, N. M.; Li, Q. Long-distance atmospheric transport of microplastic fibres influenced by their shapes. *Nat. Geosci.* **2023**, *16* (10), 863−870.

(9) Amato-Lourenço, L. F.; dos Santos Galvão, L.; de Weger, L. A.; Hiemstra, P. S.; Vijver, M. G.; Mauad, T. An emerging class of air pollutants: potential effects of microplastics to respiratory human health? *Sci. Total Environ.* **2020**, *749*, 141676.

(10) Leslie, H. A.; van Velzen, M. J. M.; Brandsma, S. H.; Vethaak, A. D.; Garcia-Vallejo, J. J.; Lamoree, M. H. Discovery and

quantification of plastic particle pollution in human blood. *Environ. Int.* **2022**, *163*, 107199.
(11) Xu, L.; Bai, X.; Li, K.; Zhang, G.; Zhang, M.; Hu, M.; Huang, Y. Human exposure to ambient atmospheric microplastics in a megacity: spatiotemporal variation and associated microorganism-related health risk. *Environ. Sci. Technol.* **2024**, *58* (8), 3702−3713.
(12) Gasperi, J.; Wright, S. L.; Dris, R.; Collard, F.; Mandin, C.; Guerrouache, M.; Langlois, V.; Kelly, F. J.; Tassin, B. Microplastics in air: are we breathing it in? *Curr. Opin. Environ. Sci. Health* **2018**, *1*, 1−5.
(13) Nihart, A. J.; Garcia, M. A.; El Hayek, E.; Liu, R.; Olewine, M.; Kingston, J. D.; Castillo, E. F.; Gullapalli, R. R.; Howard, T.; Bleske, B.; Scott, J.; Gonzalez-Estrella, J.; Gross, J. M.; Spilde, M.; Adolphi, N. L.; Gallego, D. F.; Jarrell, H. S.; Dvorscak, G.; Zuluaga-Ruiz, M. E.; West, A. B.; Campen, M. J. Bioaccumulation of microplastics in decedent human brains. *Nat. Med.* **2025**, *31*, 1114−1119.
(14) Zha, H.; Li, S.; Zhuge, A.; Shen, J.; Yao, Y.; Chang, K.; Li, L. Hazard assessment of airborne and foodborne biodegradable polyhydroxyalkanoates microplastics and non-biodegradable polypropylene microplastics. *Environ. Int.* **2025**, *196*, 109311.
(15) Aeschlimann, M.; Li, G.; Kanji, Z. A.; Mitrano, D. M. Potential impacts of atmospheric microplastics and nanoplastics on cloud formation processes. *Nat. Geosci.* **2022**, *15* (12), 967−975.
(16) Zhang, N.; Zhang, C.; Qin, Y.; Wang, J.; Ge, X.; Li, H.; Dai, Y.; Aruffo, E. A review of atmospheric microplastics: sources, characteristics, and detection method. *Curr. Pollut. Rep.* **2024**, *10* (3), 412−429.
(17) Khalid, N.; Aqeel, M.; Noman, A.; Khan, S. M.; Akhter, N. Interactions and effects of microplastics with heavy metals in aquatic and terrestrial environments. *Environ. Pollut.* **2021**, *290*, 118104.
(18) Krause, S.; Ouellet, V.; Allen, D.; Allen, S.; Moss, K.; Nel, H. A.; Manaseki-Holland, S.; Lynch, I. The potential of micro- and nanoplastics to exacerbate the health impacts and global burden of non-communicable diseases. *Cell Rep. Med.* **2024**, *5* (6), 101581.
(19) Guilhermino, L.; Vieira, L. R.; Ribeiro, D.; Tavares, A. S.; Cardoso, V.; Alves, A.; Almeida, J. M. Uptake and effects of the antimicrobial florfenicol, microplastics and their mixtures on freshwater exotic invasive bivalve Corbicula fluminea. *Sci. Total Environ.* **2018**, *622*, 1131−1142.
(20) Ma, Y.; Huang, A.; Cao, S.; Sun, F.; Wang, L.; Guo, H.; Ji, R. Effects of nanoplastics and microplastics on toxicity, bioaccumulation, and environmental fate of phenanthrene in fresh water. *Environ. Pollut.* **2016**, *219*, 166−173.
(21) Barboza, L. G. A.; Vieira, L. R.; Branco, V.; Carvalho, C.; Guilhermino, L. Microplastics increase mercury bioconcentration in gills and bioaccumulation in the liver, and cause oxidative stress and damage in Dicentrarchus labrax juveniles. *Sci. Rep.* **2018**, *8* (1), 15655.
(22) Li, C.; Gillings, M. R.; Zhang, C.; Chen, Q.; Zhu, D.; Wang, J.; Zhao, K.; Xu, Q.; Leung, P. H.; Li, X.; Liu, J.; Jin, L. Ecology and risks of the global plastisphere as a newly expanding microbial habitat. *Innovation* **2024**, *5* (1), 100543.
(23) Busse, H. L.; Ariyasena, D. D.; Orris, J.; Freedman, M. A. Pristine and aged microplastics can nucleate ice through immersion freezing. *ACS ES&T Air* **2024**, *1* (12), 1579−1588.
(24) O'Brien, S.; Rauert, C.; Ribeiro, F.; Okoffo, E. D.; Burrows, S. D.; O'Brien, J. W.; Wang, X.; Wright, S. L.; Thomas, K. V. There's something in the air: a review of sources, prevalence and behaviour of microplastics in the atmosphere. *Sci. Total Environ.* **2023**, *874*, 162193.
(25) Wang, X.; Bolan, N.; Tsang, D. C. W.; Sarkar, B.; Bradney, L.; Li, Y. A review of microplastics aggregation in aquatic environment: Influence factors, analytical methods, and environmental implications. *J. Hazard. Mater.* **2021**, *402*, 123496.
(26) Lin, Y.; Huang, X.; Liu, Q.; Lin, Z.; Jiang, G. Thermal fragmentation enhanced identification and quantification of polystyrene micro/nanoplastics in complex media. *Talanta* **2020**, *208*, 120478.
(27) Mai, L.; Bao, L. J.; Shi, L.; Wong, C. S.; Zeng, E. Y. A review of methods for measuring microplastics in aquatic environments. *Environ. Sci. Pollut. Res.* **2018**, *25*, 11319−11332.
(28) Primpke, S.; Christiansen, S. H.; Cowger, W. C.; De Frond, H.; Deshpande, A. D.; Fischer, M.; Holland, E. B.; Meyns, M.; O'Donnell, B. A.; Oßmann, B. E.; Pittroff, M.; Sarau, G.; Scholz-Böttcher, B. M.; Wiggin, K. J. J. A. S. Critical assessment of analytical methods for the harmonized and cost-efficient analysis of microplastics. *Appl. Spectrosc.* **2020**, *74*, 1012−1047.
(29) Xu, G.; Cheng, H.; Jones, R.; Feng, Y.; Gong, K.; Li, K.; Fang, X.; Tahir, M. A.; Valev, V. K.; Zhang, L. Surface-enhanced raman spectroscopy facilitates the detection of microplastics < 1 μm in the environment. *Environ. Sci. Technol.* **2020**, *54* (24), 15594−15603.
(30) Fan, W.; Salmond, J. A.; Dirks, K. N.; Cabedo Sanz, P.; Miskelly, G. M.; Rindelaub, J. D. J. E. S. Technology. Evidence and mass quantification of atmospheric microplastics in a coastal New Zealand city. *Environ. Sci. Technol.* **2022**, *56* (24), 17556−17568.
(31) Chen, Y.; Jing, S.; Wang, Y.; Song, Z.; Xie, L.; Shang, X.; Fu, H.; Yang, X.; Wang, H.; Wu, M.; Chen, Y.; Li, Q.; Zhang, Y.; Wang, W.; Zhang, L.; Wang, R.; Fang, M.; Zhang, Y.; Li, W.; Zhao, D.; Li, C.; Rudich, Y.; Wang, L.; Zhang, R.; Liu, W.; Wanger, T. C.; Yu, S.; Chen, J. Quantification and characterization of fine plastic particles as considerable components in atmospheric fine particles. *Environ. Sci. Technol.* **2024**, *58* (10), 4691−4703.
(32) Lykkemark, J.; Mattonai, M.; Vianello, A.; Gomiero, A.; Modugno, F.; Vollertsen, J. Py-GC-MS analysis for microplastics: unlocking matrix challenges and sample recovery when analyzing wastewater for polypropylene and polystyrene. *Water Res.* **2024**, *261*, 122055.
(33) Zhang, J.; Fu, D.; Feng, H.; Li, Y.; Zhang, S.; Peng, C.; Wang, Y.; Sun, H.; Wang, L. Mass spectrometry detection of environmental microplastics: Advances and challenges. *TrAC Trends Anal. Chem.* **2024**, *170*, 117472.
(34) Wang, L.; Peng, Y.; Xu, Y.; Zhang, J.; Zhang, T.; Yan, M.; Sun, H. An in situ depolymerization and liquid chromatography-tandem mass spectrometry method for quantifying polylactic acid microplastics in environmental samples. *Environ. Sci. Technol.* **2022**, *56* (18), 13029−13035.
(35) Niu, S.; Liu, R.; Zhao, Q.; Gagan, S.; Dodero, A.; Ying, Q.; Ma, X.; Cheng, Z.; China, S.; Canagaratna, M.; Zhang, Y. Quantifying the chemical composition and real-time mass loading of nanoplastic particles in the atmosphere using aerosol mass spectrometry. *Environ. Sci. Technol.* **2024**, *58* (7), 3363−3374.
(36) Tawadrous, M. A. R.; Lee, A. K. Y.; Chan, A. W. H. Characterization of airborne PET nanoplastic particles using aerosol mass spectrometry. *Aerosol Sci. Technol.* **2025**, *59* (6), 691−704.
(37) Canagaratna, M. R.; Jayne, J. T.; Jimenez, J. L.; Allan, J. D.; Alfarra, M. R.; Zhang, Q.; Onasch, T. B.; Drewnick, F.; Coe, H.; Middlebrook, A.; Delia, A.; Williams, L. R.; Trimborn, A. M.; Northway, M. J.; DeCarlo, P. F.; Kolb, C. E.; Davidovits, P.; Worsnop, D. R. Chemical and microphysical characterization of ambient aerosols with the aerodyne aerosol mass spectrometer. *Mass Spectrom. Rev.* **2007**, *26* (2), 185−222.
(38) Jayne, J. T.; Leard, D. C.; Zhang, X.; Davidovits, P.; Smith, K. A.; Kolb, C. E.; Worsnop, D. R. Development of an aerosol mass spectrometer for size and composition analysis of submicron particles. *Aerosol Sci. Technol.* **2000**, *33* (1−2), 49−70.
(39) Jimenez, J. L.; Jayne, J. T.; Shi, Q.; Kolb, C. E.; Worsnop, D. R.; Yourshaw, I.; Seinfeld, J. H.; Flagan, R. C.; Zhang, X.; Smith, K. A.; Morris, J. W.; Davidovits, P. Ambient aerosol sampling using the aerodyne aerosol mass spectrometer. *J. Geophys. Res.: Atmos.* **2003**, *108* (D7), 8425.
(40) Drewnick, F.; Hings, S. S.; DeCarlo, P.; Jayne, J. T.; Gonin, M.; Fuhrer, K.; Weimer, S.; Jimenez, J. L.; Demerjian, K. L.; Borrmann, S.; Worsnop, D. R. A new time-of-flight aerosol mass spectrometer (TOF-AMS)—Instrument description and first field deployment. *Aerosol Sci. Technol.* **2005**, *39* (7), 637−658.
(41) Wang, J.; Ge, X.; Chen, Y.; Shen, Y.; Zhang, Q.; Sun, Y.; Xu, J.; Ge, S.; Yu, H.; Chen, M. Highly time-resolved urban aerosol

https://doi.org/10.1021/acs.est.5c06513
Environ. Sci. Technol. XXXX, XXX, XXX−XXX

characteristics during springtime in yangtze river delta, china: insights from soot particle aerosol mass spectrometry. *Atmos. Chem. Phys.* **2016**, *16* (14), 9109−9127.
(42) Zhou, L.; Liang, Z.; Go, B. R.; Cuevas, R. A. I.; Tang, R.; Li, M.; Cheng, C.; Chan, C. K. Sulfate formation via aerosol-phase SO_2 oxidation by model biomass burning photosensitizers: 3,4-dimethoxybenzaldehyde, vanillin and syringaldehyde using single-particle mixing-state analysis. *Atmos. Chem. Phys.* **2023**, *23* (9), 5251−5261.
(43) Yang, Y.; Peng, X.; Zhang, G.; Hu, X.; Guo, Z.; Sun, W.; Fu, Y.; Jiang, F.; Ou, J.; Ding, X.; Wang, X.; Bi, X. In-cloud scavenging of chemically segregated particle types by individual particle observation. *Appl. Geochem.* **2023**, *152*, 105657.
(44) Li, L.; Wang, Q.; Zhang, Y.; Liu, S.; Zhang, T.; Wang, S.; Tian, J.; Chen, Y.; Hang Ho, S. S.; Han, Y.; Cao, J. Impact of reduced anthropogenic emissions on chemical characteristics of urban aerosol by individual particle analysis. *Chemosphere* **2022**, *303*, 135013.
(45) Jacobson, M. Z. Strong radiative heating due to the mixing state of black carbon in atmospheric aerosols. *Nature* **2001**, *409* (6821), 695−697.
(46) Pratt, K. A.; Prather, K. A. Real-time, single-particle volatility, size, and chemical composition measurements of aged urban aerosols. *Environ. Sci. Technol.* **2009**, *43* (21), 8276−8282.
(47) Du, X.; Xie, Q.; Huang, Q.; Li, X.; Yang, J.; Hou, Z.; Wang, J.; Li, X.; Zhou, Z.; Huang, Z.; Gao, W.; Li, L. Development and characterization of a high-performance single-particle aerosol mass spectrometer (HP-SPAMS). *Atmos. Meas. Technol.* **2024**, *17* (3), 1037−1050.
(48) Li, L.; Huang, Z.; Dong, J.; Li, M.; Gao, W.; Nian, H.; Fu, Z.; Zhang, G.; Bi, X.; Cheng, P.; Zhou, Z. Real time bipolar time-of-flight mass spectrometer for analyzing single aerosol particles. *Int. J. Mass Spectrom.* **2011**, *303* (2), 118−124.
(49) DeCarlo, P. F.; Kimmel, J. R.; Trimborn, A.; Northway, M. J.; Jayne, J. T.; Aiken, A. C.; Gonin, M.; Fuhrer, K.; Horvath, T.; Docherty, K. S.; Worsnop, D. R.; Jimenez, J. L. Field-deployable, high-resolution, time-of-flight aerosol mass spectrometer. *Anal. Chem.* **2006**, *78* (24), 8281−8289.
(50) Canagaratna, M. R.; Jayne, J. T.; Jimenez, J. L.; Allan, J. D.; Alfarra, M. R.; Zhang, Q.; Onasch, T. B.; Drewnick, F.; Coe, H.; Middlebrook, A.; Delia, A.; Williams, L. R.; Trimborn, A. M.; Northway, M. J.; DeCarlo, P. F.; Kolb, C. E.; Davidovits, P.; Worsnop, D. R. Chemical and microphysical characterization of ambient aerosols with the aerodyne aerosol mass spectrometer. *Mass Spectrom. Rev.* **2007**, *26* (2), 185−222.
(51) Chen, Q.; Miyazaki, Y.; Kawamura, K.; Matsumoto, K.; Coburn, S.; Volkamer, R.; Iwamoto, Y.; Kagami, S.; Deng, Y.; Ogawa, S.; Ramasamy, S.; Kato, S.; Ida, A.; Kajii, Y.; Mochida, M. Characterization of chromophoric water-soluble organic matter in urban, forest, and marine aerosols by HR-ToF-AMS Analysis and excitation-emission matrix spectroscopy. *Environ. Sci. Technol.* **2016**, *50* (19), 10351−10360.
(52) Thomson, D. S.; Middlebrook, A. M.; Murphy, D. M. Thresholds for laser-induced ion formation from aerosols in a vacuum using ultraviolet and vacuum-ultraviolet laser wavelengths. *J. Aerosol Sci.* **1997**, *26* (6), 544−559.
(53) Zelenyuk, A.; Yang, J.; Choi, E.; Imre, D. SPLAT II: an aircraft compatible, ultra-sensitive, high precision instrument for in-situ characterization of the size and composition of fine and ultrafine particles. *Aerosol Sci. Technol.* **2009**, *43* (5), 411−424.
(54) Silva, P. J.; Prather, K. A. Interpretation of mass spectra from organic compounds in aerosol time-of-flight mass spectrometry. *Anal. Chem.* **2000**, *72* (15), 3553−3562.
(55) Campbell, J. M.; Vestal, M. L.; Blank, P. S.; Stein, S. E.; Epstein, J. A.; Yergey, A. L. Fragmentation of leucine enkephalin as a function of laser fluence in a MALDI TOF-TOF. *J. Am. Soc. Mass Spectrom.* **2007**, *18* (4), 607−616.
(56) Thomson, D. S.; Murphy, D. M. Laser-induced ion formation thresholds of aerosol particles in a vacuum. *Appl. Opt.* **1993**, *32* (33), 6818−6826.
(57) Wang, G.; Ruser, H.; Schade, J.; Passig, J.; Adam, T.; Dollinger, G.; Zimmermann, R. Machine learning approaches for automatic classification of single-particle mass spectrometry data. *Atmos. Meas. Technol.* **2024**, *17* (1), 299−313.
(58) Song, K.; Tang, R.; Zhang, J.; Wan, Z.; Zhang, Y.; Hu, K.; Gong, Y.; Lv, D.; Lu, S.; Tan, Y.; Zhang, R.; Li, A.; Yan, S.; Yan, S.; Fan, B.; Zhu, W.; Chan, C. K.; Yao, M.; Guo, S. Molecular fingerprints and health risks of smoke from home-use incense burning. *Atmos. Chem. Phys.* **2023**, *23* (21), 13585−13595.
(59) Silva, P. J.; Liu, D.-Y.; Noble, C. A.; Prather, K. A. Size and Chemical Characterization of individual particles resulting from biomass burning of local southern california species. *Environ. Sci. Technol.* **1999**, *33* (18), 3068−3076.
(60) Zhou, L.; Liang, Z.; Go, B. R.; Cuevas, R. A. I.; Tang, R.; Li, M.; Cheng, C.; Chan, C. K. Sulfate formation via aerosol-phase SO_2 oxidation by model biomass burning photosensitizers: 3,4-dimethoxybenzaldehyde, vanillin and syringaldehyde using single-particle mixing-state analysis. *Atmos. Chem. Phys.* **2023**, *23* (9), 5251−5261.
(61) Edwards, K. C.; Kapur, S.; Fang, T.; Cesler-Maloney, M.; Yang, Y.; Holen, A. L.; Wu, J.; Robinson, E. S.; DeCarlo, P. F.; Pratt, K. A.; Weber, R. J.; Simpson, W. R.; Shiraiwa, M. Residential wood burning and vehicle emissions as major sources of environmentally persistent free radicals in fairbanks, Alaska. *Environ. Sci. Technol.* **2024**, *58* (32), 14293−14305.
(62) Zhang, Y.; Pei, C.; Zhang, J.; Cheng, C.; Lian, X.; Chen, M.; Huang, B.; Fu, Z.; Zhou, Z.; Li, M. Detection of polycyclic aromatic hydrocarbons using a high performance-single particle aerosol mass spectrometer. *J. Environ. Sci.* **2023**, *124*, 806−822.
(63) Kirchsteiger, B.; Materić, D.; Happenhofer, F.; Holzinger, R.; Kasper-Giebl, A. Fine micro- and nanoplastics particles ($PM_{2.5}$) in urban air and their relation to polycyclic aromatic hydrocarbons. *Atmos. Environ.* **2023**, *301*, 119670.
(64) Shahzad, K.; Hasan, A.; Hussain Naqvi, S. K.; Parveen, S.; Hussain, A.; Ko, K.-C.; Park, S. H. Recent advances and factors affecting the adsorption of nano/microplastics by magnetic biochar. *Chemosphere* **2025**, *370*, 143936.
(65) You, X.; Cao, X.; Zhang, X.; Guo, J.; Sun, W. Unraveling individual and combined toxicity of nano/microplastics and ciprofloxacin to *Synechocystis* sp. at the cellular and molecular levels. *Environ. Int.* **2021**, *157*, 106842.
(66) Brüggemann, M.; Xu, R.; Tilgner, A.; Kwong, K. C.; Mutzel, A.; Poon, H. Y.; Otto, T.; Schaefer, T.; Poulain, L.; Chan, M. N.; Herrmann, H. Organosulfates in ambient aerosol: state of knowledge and future research directions on formation, abundance, fate, and importance. *Environ. Sci. Technol.* **2020**, *54* (7), 3767−3782.
(67) Rudich, Y.; Donahue, N. M.; Mentel, T. F. Aging of Organic Aerosol: Bridging the Gap Between Laboratory and Field Studies. *Annu. Rev. Phys. Chem.* **2007**, *58*, 321−352.
(68) Jiang, F.; Zheng, Z.; Coe, H.; Healy, R. M.; Poulain, L.; Gros, V.; Zhang, H.; Li, W.; Liu, D.; West, M.; Topping, D.; Riemer, N. Integrating simulations and observations: a foundation model for estimating the aerosol mixing state index. *ACS ES&T Air* **2025**, *2* (5), 877−890.
(69) Li, X.; Li, L.; Zhuo, Z.; Zhang, G.; Du, X.; Li, X.; Huang, Z.; Zhou, Z.; Cheng, Z. Bioaerosol identification by wide particle size range single particle mass spectrometry. *Atmosphere* **2023**, *14* (6), 1017.

https://doi.org/10.1021/acs.est.5c06513
Environ. Sci. Technol. XXXX, XXX, XXX−XXX